

Sbi00515, a Protein of Unknown Function from *Streptomyces bingchenggensis*, Highlights the Functional Versatility of the Acetoacetate Decarboxylase Scaffold

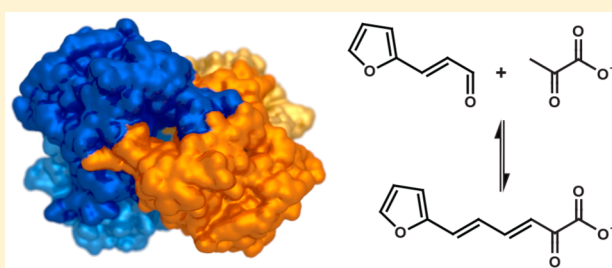
Lisa S. Mueller, Robert W. Hoppe, Jenna M. Ochsenwald, Robert T. Berndt, Geoffrey B. Severin, Alan W. Schwabacher, and Nicholas R. Silvaggi*

Department of Chemistry and Biochemistry, University of Wisconsin—Milwaukee, 3210 North Cramer Street, Milwaukee, Wisconsin 53211, United States

S Supporting Information

ABSTRACT: The acetoacetate decarboxylase-like superfamily (ADCSF) is a group of ~4000 enzymes that, until recently, was thought to be homogeneous in terms of the reaction catalyzed. Bioinformatic analysis shows that the ADCSF consists of up to seven families that differ primarily in their active site architectures. The soil-dwelling bacterium *Streptomyces bingchenggensis* BCW-1 produces an ADCSF enzyme of unknown function that shares a low level of sequence identity (~20%) with known acetoacetate decarboxylases (ADCs). This enzyme, Sbi00515, belongs to the MppR-like family of the ADCSF

because of its similarity to the mannopeptimycin biosynthetic protein MppR from *Streptomyces hygroscopicus*. Herein, we present steady state kinetic data that show Sbi00515 does not catalyze the decarboxylation of any α - or β -keto acid tested. Rather, we show that Sbi00515 catalyzes the condensation of pyruvate with a number of aldehydes, followed by dehydration of the presumed aldol intermediate. Thus, Sbi00515 is a pyruvate aldolase-dehydratase and not an acetoacetate decarboxylase. We have also determined the X-ray crystal structures of Sbi00515 in complexes with formate and pyruvate. The structures show that the overall fold of Sbi00515 is nearly identical to those of both ADC and MppR. The pyruvate complex is trapped as the Schiff base, providing evidence that the Schiff base chemistry that drives the acetoacetate decarboxylases has been co-opted to perform a new function, and that this core chemistry may be conserved across the superfamily. The structures also suggest possible catalytic roles for several active site residues.



The acetoacetate decarboxylase-like superfamily (ADCSF; IPR010451, IPR023375, and IPR023653) is a largely unstudied group of approximately 4000 proteins. The superfamily member that has been most thoroughly characterized is the prototypical ADCSF enzyme, acetoacetate decarboxylase from *Clostridium acetobutylicum* (CaADC). This enzyme catalyzes the cleavage of acetoacetate to acetone and CO_2 using a Schiff base mechanism involving a catalytic lysine residue.^{1–5} To date, most members of the ADCSF are annotated as either acetoacetate decarboxylases, often on the basis of a relatively low level of sequence identity, or unknown/conserved hypothetical proteins.

Previous studies have shown that, while ADCSF enzymes appear to be structurally homogeneous [e.g., CaADC (PDB entry 3BH2), *Chromobacterium violaceum* ADC (PDB entry 3BH3), *Legionella pneumophila* ADC (PDB entry 3C8W), *Methanoculleus marisnigri* ADC (PDB entry 3CMB), *Streptomyces hygroscopicus* MppR (PDB entry 4JM3), and Sbi00515 (PDB entry 4ZBO, this study)], there is some diversity in terms of the substrates used and the chemistry catalyzed by members of this superfamily.⁶ MppR from *S. hygroscopicus* (ShMppR), for example, was observed in X-ray diffraction experiments to catalyze the cyclization of 2-oxo-4-hydroxy-5-guanidinovaleric

acid (i.e., “4-hydroxy-ketoarginine”) to give what would become, after hydrolysis from the enzyme, the keto form of the nonproteinogenic amino acid enduracidine.⁶ While the precise role of ShMppR in the biosynthesis of enduracidine remains unclear, it is apparent that very little is known about the degree of substrate and reaction diversity within the ADCSF.

Not surprisingly, the divergence of ShMppR's catalytic activity from the classical acetoacetate decarboxylases like CaADC is associated with a number of amino acid substitutions in the active site. Chief among these are the loss of an Arg side chain proposed to orient the substrate for decarboxylation in CaADC, loss of the “second Glu” side chain thought to promote decarboxylation in CaADC,³ and an increase in polarity in the neighborhood of the catalytic Lys in ShMppR. This latter change results in the formation of an α -carboxylate-binding site in MppR.⁶ Comparative genome analysis of ShMppR and closely related homologues showed that there exists a subset of ADCSF enzymes that share this same pattern of amino acid substitutions

Received: May 1, 2015

Revised: June 2, 2015

Published: June 3, 2015

Table 1. Steady State Kinetic Parameters Measured for the Reaction of 2.0 μ M Sbi00515 with the Enone Substrate 1 in the Absence of Pyruvate or in the Presence of Saturating Concentrations of Pyruvate (50 mM) and Various Aldehyde Substrates (see Schemes 1 and 2), Subsaturating Concentrations of 2 (50 mM) and Pyruvate (3), or Saturating Concentrations of 10 (10 mM) and Pyruvate^a

substrate	k_{cat} (s^{-1})	K_{M} (mM)	$k_{\text{cat}}/K_{\text{M}}$ ($\text{M}^{-1} \text{s}^{-1}$)	product	
				λ_{mon} (nm)	ϵ ($\text{M}^{-1} \text{cm}^{-1}$)
benzylidene-pyruvate (1)	1.2 ± 0.20	22.3 ± 7.0	5.4×10^1	300	24159
benzaldehyde (2)	3.2 ± 0.16	51.5 ± 6.1	6.2×10^1	300	11426
4-hydroxybenzaldehyde (4)	0.01 ± 0.001	0.4 ± 0.05	2.5×10^1	360	1217
<i>trans</i> -2-pentenal (5)	1.2 ± 0.05	6.6 ± 0.4	1.8×10^2	290	26021
<i>trans</i> -2-hexenal (6)	12.9 ± 0.6	1.8 ± 0.1	7.2×10^3	290	8576
hexanal (7)	no reaction	—	—	—	—
2,4-heptadienal (8)	0.90 ± 0.04	0.3 ± 0.02	3.0×10^3	360	2432
3,7-dimethyl-2,6-octadienal (citral, 9)	0.28 ± 0.01	0.04 ± 0.002	7.0×10^3	330	3393
<i>trans</i> -3-(2-furyl)acrolein (10)	22.9 ± 0.8	1.2 ± 0.08	1.9×10^4	390	10062
pyruvate (3) ^b	1.75 ± 0.07	17.2 ± 2.8	1.0×10^2	300	—
pyruvate (3) ^c	22.5 ± 1.2	11.8 ± 1.6	1.9×10^3	390	—

^aAs described in the text, the poor binding and limited solubility of 2 made it impossible to fully saturate the enzyme. The kinetic parameters apply to the substrate in column 1. The extinction coefficients given are for benzylidene-pyruvate itself (row 1) and the condensation products of pyruvate with the aldehyde substrates tested (remaining rows). ^bBecause of the high K_{M} value for 2, reaction mixtures were not saturated with respect to this substrate. ^cReaction kinetics of pyruvate with 10 were nearly saturated (the concentration of 10 was \sim 10-fold greater than the measured K_{M} value).

in the active site. These so-called MppR-like enzymes comprise one of seven sequence clusters or families within the ADCSF.

Herein, we describe the structure and biochemical characterization of one of these MppR-like enzymes, Sbi00515 from *Streptomyces bingchenggensis* BCW-1. *S. bingchenggensis* is notable not only for the sheer size of its genome [at \sim 12 million bp (10106 genes),⁷ it is one of the largest bacterial genomes known] but also for the number of secondary metabolites it produces. These include the antihelminthic milbamyins A3 and A4 that are used extensively to control worms in animals, 10 additional milbemycin analogues,^{8–11} the polyether antibiotic nanchangmycin, the antitumor agents bingchamide A and B,¹² and at least 23 uncharacterized nonribosomal peptide, polyketide, or terpene biosynthetic clusters.⁷ The gene encoding Sbi00515 is near one of the uncharacterized polyketide synthase genes, raising the possibility that Sbi00515 has some role in synthesizing an as-yet-unknown natural product.

MATERIALS AND METHODS

Cloning, Expression, and Purification of Sbi00515. The coding sequence of gene product Sbi00515 was optimized for expression in *Escherichia coli* and synthesized by GenScript Inc. (Piscataway, NJ). This synthetic gene was subcloned into the pE-SUMO_{kan} expression vector (LifeSensors Inc., Malvern, PA) using primers containing BsaI and XbaI restriction sites (forward, 5'-GGTCTCAAGGTATGAAAGGTTATACGGTTCGG-3'; reverse, 5'-GCTCTAGATCATCATGCCGAATGGTCTGC-3'). The His₆-tagged SUMO–Sbi00515 fusion protein was expressed from *E. coli* BL21 Star (DE3) cells (Invitrogen Inc., Carlsbad, CA) carrying the pE-SUMO-Sbi00515 plasmid. Cultures were grown in Luria-Bertani medium with 50 μ g/mL kanamycin at 37 °C. At an OD₆₀₀ of \sim 0.9, protein expression was induced with 0.4 mM IPTG. The temperature was reduced to 25 °C, and the cultures were grown overnight while being shaken at 250 rpm. Cells were harvested by centrifugation, resuspended in 5 mL/g of buffer A [25 mM Tris (pH 8.0), 300 mM NaCl, and 10 mM imidazole] supplemented with 1 mg/mL hen egg lysozyme (Hampton Research) and frozen at -20 °C. Cells were lysed by thawing the resuspended cells for 2 h at room temperature (RT), after which DNase I (Worthington Biochemical Corp., Lakewood, NJ) was added to achieve a concentration of 0.1 mg/mL.

The lysate was clarified by centrifugation at 39000g for 45 min and then applied to a 5 mL HisTrap column (GE Lifesciences, Piscataway, NJ) at a flow rate of 5 mL/min to isolate the His₆-SUMO–Sbi00515 fusion protein. The protein was eluted by a four-step gradient of buffer B [25 mM Tris (pH 8.0), 300 mM NaCl, and 250 mM imidazole (5, 15, 50, and 100%)]. The His₆-SUMO–Sbi00515 fusion protein eluted in the third and fourth steps and was \sim 90% pure, as judged on Coomassie-stained sodium dodecyl sulfate–polyacrylamide gel electrophoresis gels. Peak fractions were pooled and dialyzed overnight against 3.5 L of 25 mM Tris (pH 8.0) and 150 mM NaCl in the presence of \sim 3 μ M SUMO protease (LifeSensors Inc.). The dialysate was passed through the HisTrap column a second time to remove the cleaved His₆-SUMO tag as well as the protease. The resulting Sbi00515 preparation was $>$ 95% pure. Selenomethionine-labeled Sbi00515 was purified using the same protocol, except that SelenoMethionine Medium Complete (Molecular Dimensions, Newmarket, Suffolk, U.K.) was used as the growth medium rather than Luria-Bertani broth and T7 Express Crystal cells (New England Biolabs, Ipswich, MA) were used in place of the BL21 Star (DE3) cells.

Preparation of Benzylidenepyruvate (1). (*E*)-2-Oxo-4-phenylbut-3-enoic acid (1) was prepared by a modification of the technique of Reimer.¹³ A suspension of benzaldehyde (5.22 g, 49.2 mmol), sodium pyruvate (5.42 g, 49.3 mmol), and KOH (1.41 g, 25.2 mmol) in 15 mL of CH₃OH and 15 mL of H₂O was warmed from <10 to 35 °C and held at that temperature for 1.5 h, over which time the starting materials dissolved, and then the product crystallized. Filtration, rinsing with 50 mL of cold CH₃OH, and drying *in vacuo* gave 5.25 g of a yellow solid. A solution of 5.18 g of the yellow solid in 150 mL of H₂O was filtered and acidified with HCl (2.0 M, 180 mL), and the resulting precipitate was isolated by filtration and then dried by addition and rotary evaporation of 50 mL of toluene *in vacuo* to yield 2.91 g of product as an orange solid (34% yield). The ¹H and ¹³C NMR spectra of this product were identical to those reported previously.¹⁴

Steady State Enzyme Kinetics. All 0.5 mL kinetic assays were conducted in triplicate at 25 °C in 50 mM Bis-Tris (pH 7.0). The initial velocity of Sbi00515-catalyzed hydrolysis of 1 was measured directly by monitoring the decrease in absorbance

Table 2. Crystallographic Data Collection and Model Refinement Statistics

	SeMet Sbi00515	native Sbi00515	Sbi00515-pyruvate
resolution (Å) (last shell) ^a	46.5–1.9 (1.97–1.90)	41.58–1.4 (1.45–1.40)	39.9–1.8 (1.86–1.80)
wavelength (Å)	0.97921	0.97896	1.54180
no. of reflections			
observed	1131019 (96476)	1626413 (91229)	285228 (8521)
unique	82988 (8183)	207128 (20393)	92300 (6104)
completeness (%) ^a	100.0 (100.0)	99.9 (99.5)	95.4 (64.0)
<i>R</i> _{merge} (%) ^{a,b}	0.145 (0.456)	0.071 (0.560)	0.102 (0.334)
multiplicity	13.6 (11.8)	7.9 (4.5)	3.1 (1.4)
$\langle I/\sigma(I) \rangle$ ^a	22.3 (5.9)	20.5 (2.2)	12.3 (1.7)
figure of merit (acentric)	0.283		
phasing power	1.102		
Model Refinement			
no. of reflections in the work set	78722	207021	92221
no. of reflections in the test set	4185	2960	4631
<i>R</i> _{cryst} (<i>R</i> _{free})	0.162 (0.185)	0.154 (0.176)	0.163 (0.205)
no. of residues	1023	1034	1028
no. of solvent atoms	1166	1385	1289
no. of TLS groups	24	25	25
average <i>B</i> factor (Å ²) ^c			
protein atoms	15.9	21.0	21.4
ligand atoms	35.6	33.9	31.9
solvent	26.9	34.1	31.3
root-mean-square deviation			
bond lengths (Å)	0.005	0.009	0.011
bond angles (deg)	0.979	1.303	1.309
coordinate error (Å)	0.30	0.12	0.18
Ramachandran statistics (favored/allowed/outliers)	98.2/1.8/0	97.7/2.3/0	97.2/2.8/0

^aValues in parentheses apply to the high-resolution shell indicated in the resolution row. ^b $R = \sum(|F_{\text{obs}}| - \text{scale} \times |F_{\text{calc}}|) / \sum |F_{\text{obs}}|$. ^cIsotropic equivalent *B* factors, including the contribution from TLS refinement.

at 330 nm. Likewise, initial velocities of Sbi00515-catalyzed condensation of pyruvate with various aldehyde substrates was also monitored directly. Extinction coefficients and optimal wavelengths for monitoring the reactions are listed in Table 1. The extinction coefficients were determined empirically by comparing appropriate peaks in the proton NMR spectra of the various enone products produced in the condensation reactions with the peak for the α -proton of tryptophan (added to the NMR samples as a standard) to estimate the concentration of the product. The tryptophan stock concentration was calculated from the absorbance at 280 nm and the known extinction coefficient (5540 M⁻¹ cm⁻¹).¹⁵ The *k*_{cat} and *K*_M values were determined from the initial velocity data using the equation $v_0 = V_m[A]/(K_M + [A])$, where [A] is the concentration of the aldehyde or benzylidenepyruvate substrate, *v*₀ is the initial velocity, *V*_m is the maximal velocity, and *K*_M is the Michaelis constant.

High-Performance Liquid Chromatography (HPLC) Analysis of Sbi00515 Reaction Mixtures. Reaction mixtures (500 μ L) containing 12.3 mM **1** in 50 mM sodium phosphate (pH 7.4) and 5.7 μ M enzyme, as well as authentic standards of **1** and **2**, were separated using a 50 mm \times 2.0 mm, 2.5 μ m Synergy Polar RP column (Phenomenex) on an Agilent 1220 HPLC system. The gradient ran from 5 to 50% acetonitrile in a 0.1% TFA/water mixture over 8 min at a flow rate of 0.5 mL/min. Analytes were detected by absorbance at 260 nm. All samples were incubated for 50 min at RT before being passed through 10K molecular weight cutoff centrifugal filter devices to remove the enzyme.

¹H NMR Analysis of Sbi00515 Reaction Mixtures.

Reaction mixtures (500 μ L) contained 2.8 μ M Sbi00515 and 12.5 mM **1** or 50 mM **2** with 50 mM pyruvate in 50 mM sodium phosphate buffer (pH 7.4) (H₂O). The reaction mixtures were incubated at RT for 80 min (**1**) or 35 min (**2** with pyruvate), after which the samples were evaporated to dryness in a CentriFan centrifugal evaporator. The residues were resuspended in 500 μ L of D₂O. NMR spectra were recorded at RT on a Bruker DRX500 500 MHz spectrometer equipped with a BBI probe. All data sets consist of 128 scans. Standard samples of **1** (12.5 mM) and the mixture of **2** with pyruvate (50 mM each) were treated in the same way as the enzymatic reaction mixtures.

Crystallization, Structure Determination, and Model Refinement. Initial crystallization conditions were identified by screening 45 mg/mL Sbi00515 against the Index HT screen (Hampton Research). After optimization, diffraction-quality crystals were obtained by the hanging drop vapor diffusion method from 3.5–3.7 M potassium formate, 2–3% polyethylene glycol monomethyl ether 2000 (PEG MME 2K), and 100 mM bis-Tris propane (pH 9.0). Drops contained 1–2 μ L of a protein solution at 45 mg/mL and 1 μ L of a crystallization solution. Crystals formed as plates that appeared after 3–4 days and grew to maximal dimensions of \sim 800 μ m \times 200 μ m \times 50 μ m. Crystals of selenomethionine (SeMet)-substituted Sbi00515 were grown using the same conditions. Crystals were cryoprotected with Paratone N (Hampton Research) and flashed-cooled by being plunged into liquid nitrogen. The structure of Sbi00515 with pyruvate bound was obtained by transferring crystals of native Sbi00515 into 30 μ L drops of a soaking solution containing 4.0 M potassium formate, 3% PEG MME 2K, 100 mM bis-Tris propane

(pH 9.0), and 30 mM sodium pyruvate. After soaking overnight, crystals were treated with Paratone N and flash-cooled. X-ray diffraction data for SeMet Sbi00515 and a higher-resolution native data set were collected at beamline 21-ID-D of the Life Science Collaborative Access Team (LS-CAT) at the Advanced Photon Source (APS). The Sbi00515-pyruvate data set was collected using the rotating anode X-ray source at Marquette University. Data were processed with HKL2000¹⁶ or MOSFLM^{17,18} and SCALA¹⁹ of the CCP4 Program Suite.²⁰

The structure of Sbi00515 was determined by the single-wavelength anomalous diffraction (SAD) method using 1.9 Å resolution data collected from a crystal of SeMet-substituted Sbi00515 at 0.97921 Å, 4.0 eV above the tabulated K-edge wavelength for Se (0.97950 Å). The program autoSHARP²¹ was used to determine the Se substructure, which contained 16 of the 24 Se atoms in the asymmetric unit, and calculate density-modified electron density maps. An initial model comprising ~75% of the asymmetric unit contents was built automatically using the PHENIX package (phenix.autobuild^{22,23}). After iterative cycles of manual model building in COOT²⁴ and maximum likelihood-based refinement using the PHENIX package (phenix.refine²⁵), ordered solvent molecules were added automatically in phenix.refine and culled manually in COOT. Hydrogen atoms were added to the model using phenix.reduce²⁶ and were included in the later stages of refinement to improve the stereochemistry of the model. Positions of H atoms were refined using the riding model with a global *B* factor. Regions of the model for translation-libration-screw (TLS) refinement were identified using phenix.find_tls_groups, and the TLS parameters were refined in phenix.refine. Once the refinement converged (e.g., for SeMet Sbi00515, *R* = 0.162 and *R*_{free} = 0.185), the model was validated using the tools implemented in COOT and PHENIX.^{27,28} Sections of the backbone with missing or uninterpretable electron density were not included in the final model. Side chains with poor or missing electron density were modeled in favored rotameric conformations. The *B* factors were allowed to refine without additional restraints, and the occupancies for atoms in all residues without alternate conformations were held to be 1.0.

The final, refined model of SeMet Sbi00515, stripped of water molecules and H atoms, and with all *B* factors set to 20.0 Å², was used to determine the structures of Sbi00515 “unliganded” (with formate bound) and with pyruvate bound by difference Fourier. A similar refinement protocol was used for both models presented here. In the case of the Sbi00515-pyruvate structure, restraints for the link between Lys122 and pyruvate were generated with phenix.elbow.²⁹ Data collection and model refinement statistics are listed in Table 2. Coordinates and structure factors have been deposited in the Protein Data Bank as entries 4ZBO and 4ZBT.

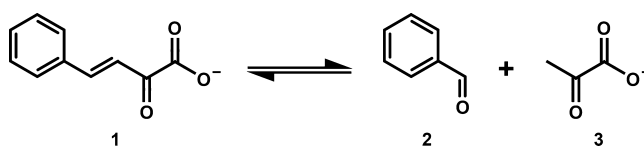
RESULTS AND DISCUSSION

Sbi00515 was chosen for study on the basis of its sequence similarity to ShMppR (39% identity) and its gene context, which suggests a potential role in an uncharacterized polyketide biosynthetic cluster (Table S1 of the Supporting Information). Because of intellectual property concerns, attempts to obtain samples of live cells or genomic DNA were unsuccessful. As such, the precise biological function of Sbi00515 cannot currently be verified. In the absence of this information, the purpose of this study was to investigate the catalytic capacity of the MppR-like family specifically, and the ADCSF in general.

Enzymatic Activity of Sbi00515. Sbi00515 was first assayed for acetoacetate decarboxylase activity as described by Highbarger et al.² Because Sbi00515 shares the same active site residue changes relative to CaADC that were observed in ShMppR, it was not surprising that it did not react with acetoacetate. As ShMppR was shown to react with pyruvate, a number of α -keto acids, including glyoxylate, pyruvate, oxaloacetate, and α -ketoglutarate, were tested as substrates for Sbi00515. While glyoxylate, pyruvate, and α -ketoglutarate were observed to form Schiff base complexes in X-ray diffraction experiments (see the discussion of the pyruvate complex below), and the enzyme binds pyruvate with a *K*_D of 5.7 ± 0.6 mM (as measured by fluorescence titration), none of these were altered by the enzyme (e.g., decarboxylated) as judged from HPLC analysis of reaction mixtures (data not shown).

The similarity of the Sbi00515 structure to that of ShMppR (see below) suggested that it should be able to react with α -keto acids. Sbi00515 was tested for activity with benzylidene pyruvate [1 (Scheme 1)], because any reaction resulting in modification of

Scheme 1



the double bond (e.g., hydration) would disrupt the chromophore and be accompanied by a change in the UV–vis absorbance spectrum. UV–vis spectroscopy (Figure 1A) showed that incubation of 1 with Sbi00515 resulted in the time-dependent loss of absorbance at 300 nm and a concomitant increase in absorbance at 254 nm. The structure of 1 and the rise of a species absorbing at 254 nm suggested that 1 was being hydrolyzed to give benzaldehyde (2) and pyruvate [3 (Scheme 1)]. The fact that these were products of the reaction was confirmed by HPLC analysis of reaction mixtures compared to authentic standards (Figure 1B) and by ¹H NMR spectroscopy (Figure 1C and Figures S1–S4 of the Supporting Information). These data clearly indicate that Sbi00515 was able to hydrate the double bond of 1 and catalyze the retro-aldol cleavage to give benzaldehyde and pyruvate. This same reaction has been observed in the *trans*-*o*-hydroxybenzylidenepyruvate hydratase-aldolase from *Pseudomonas fluorescens*,^{30,31} though this enzyme appears, from secondary structure prediction, to have the TIM-barrel fold typical of Schiff base-forming aldolases.

Because these end-point assays were conducted over relatively long time periods (30–120 min), it was possible that the reaction observed was cryptic and did not represent the physiological activity of the enzyme. To address this question, both the hydrolysis and condensation reactions were characterized by steady state enzyme kinetics. Though the reactions are clearly catalytic, the modest values of the pseudo-second-order rate constants of 54, 62, and 100 M^{−1} s^{−1} when 1, 2, and 3 are varied, respectively (Table 1), suggested either that these compounds are nonideal substrates that participate in a facsimile of the native reaction for this enzyme or that they induce nonphysiological chemistry that is only evidence of reaction promiscuity.

To clarify this point, a number of additional aldehyde substrates (Scheme 2) were screened for activity with saturating pyruvate (Table 1). Interestingly, 4-hydroxybenzaldehyde (4) has a pseudo-second-order rate constant comparable to that of 2;

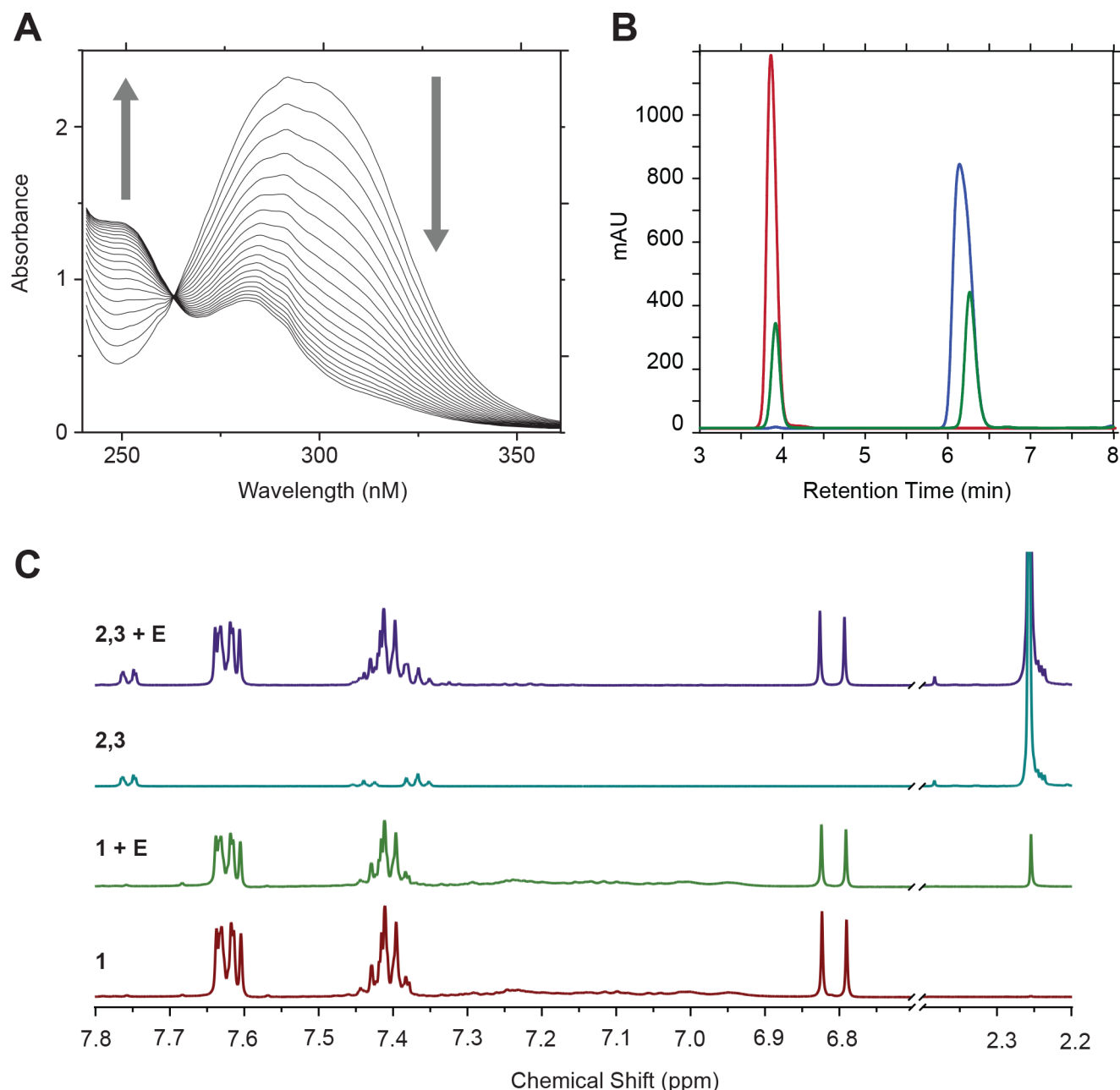
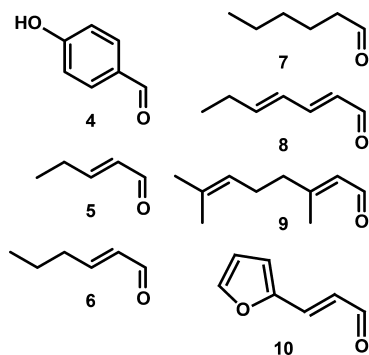


Figure 1. (A) Sbi00515-catalyzed cleavage of **1** observed by UV–vis spectroscopy. The spectra are separated by 4.5 min and thus cover a 90 min period. The 500 μ L reaction mixture contained 100 mM **1** and 12.8 μ M Sbi00515 in 10 mM MES (pH 6.0). The reaction was initiated by the addition of enzyme. (B) HPLC analysis of reaction mixtures and authentic benzaldehyde (**2**) suggests that Sbi00515 catalyzes the hydrolysis of **1** to give **2** and pyruvate (**3**). Starting material (**1**, blue trace) and benzaldehyde, the putative product (**2**, red trace), are very well resolved, eluting at 6.3 and 3.9 min, respectively. A sample containing 12.3 mM **1** and 5.7 μ M Sbi00515 (green trace) clearly shows a loss of starting material with corresponding accumulation of a product that also elutes at 3.9 min under these conditions. (C) Proton NMR spectra of reaction mixtures and standards confirm that the products of the reaction between Sbi00515 and **1** are **2** and pyruvate. The authentic starting material (**1**, red trace) gives a spectrum that is distinct from that of benzaldehyde (cyan trace). The doublet at 6.8 ppm is characteristic of the unsaturated bond. The methyl protons of pyruvate give a singlet at 2.25 ppm (cyan trace). After incubation with the enzyme, pyruvate is clearly present (green trace). Given 50 mM pyruvate, the reaction can be run in reverse (purple trace), where the doublet at 6.8 ppm confirms the production of **1**. Together, these data confirm that Sbi00515 has *in vitro* aldolase-dehydratase activity. The complete NMR spectra are provided in Figures S1–S4 of the Supporting Information.

however, the K_M value is approximately 200-fold less than that of **2**, and k_{cat} is more than 300-fold slower. This may indicate that Sbi00515 binds **4** more tightly, but in an orientation that is less favorable for catalysis. Moving from the aryl aldehyde **2** to aliphatic aldehydes **5**–**9** results in a marked improvement in K_M with small decreases in k_{cat} , such that the catalytic efficiency improves by as much as 2 orders of magnitude. There is a clear

trend of decreasing K_M with increasing chain length going from 6.6 ± 0.4 mM for **5** to 35.0 ± 2.0 μ M for **9**. There is no clear relationship between substrate size and the k_{cat} values. The complete lack of activity with **7**, as judged by HPLC analysis, shows that the unsaturated bond adjacent to the aldehyde group is required for the observed catalysis. The aromatic aldehyde 3-(2-furyl)acrolein (**10**) was chosen because it combines a short,

Scheme 2



unsaturated alkyl chain with an aromatic group. This substrate was significantly more efficient than any of the other substrates tested with a k_{cat} value of $22.9 \pm 0.8 \text{ s}^{-1}$ and a K_M value of $1.2 \pm 0.1 \text{ mM}$, for a pseudo-second-order rate constant of $1.9 \times 10^4 \text{ M}^{-1} \text{ s}^{-1}$. It is interesting to note that the diene substrate **8** reacts 20-fold more slowly than **10** despite the high degree of similarity of their structures. The ability of the furan ring to accept a hydrogen bond and/or stack with an aromatic side chain in the active site may result in **10** binding in a more favorable orientation for catalysis. Finally, the relatively robust activity with **10** does suggest that the aldol condensation and dehydration activity of Sbi00515 is real, and not a spurious reaction resulting from the presence of a reactive enamine in the active site. It should also be noted that the aldol condensation activity was observed with only pyruvate; other α -keto acids that were tested (glyoxylate, 2-oxobutyrate, oxaloacetate, and α -ketoglutarate)

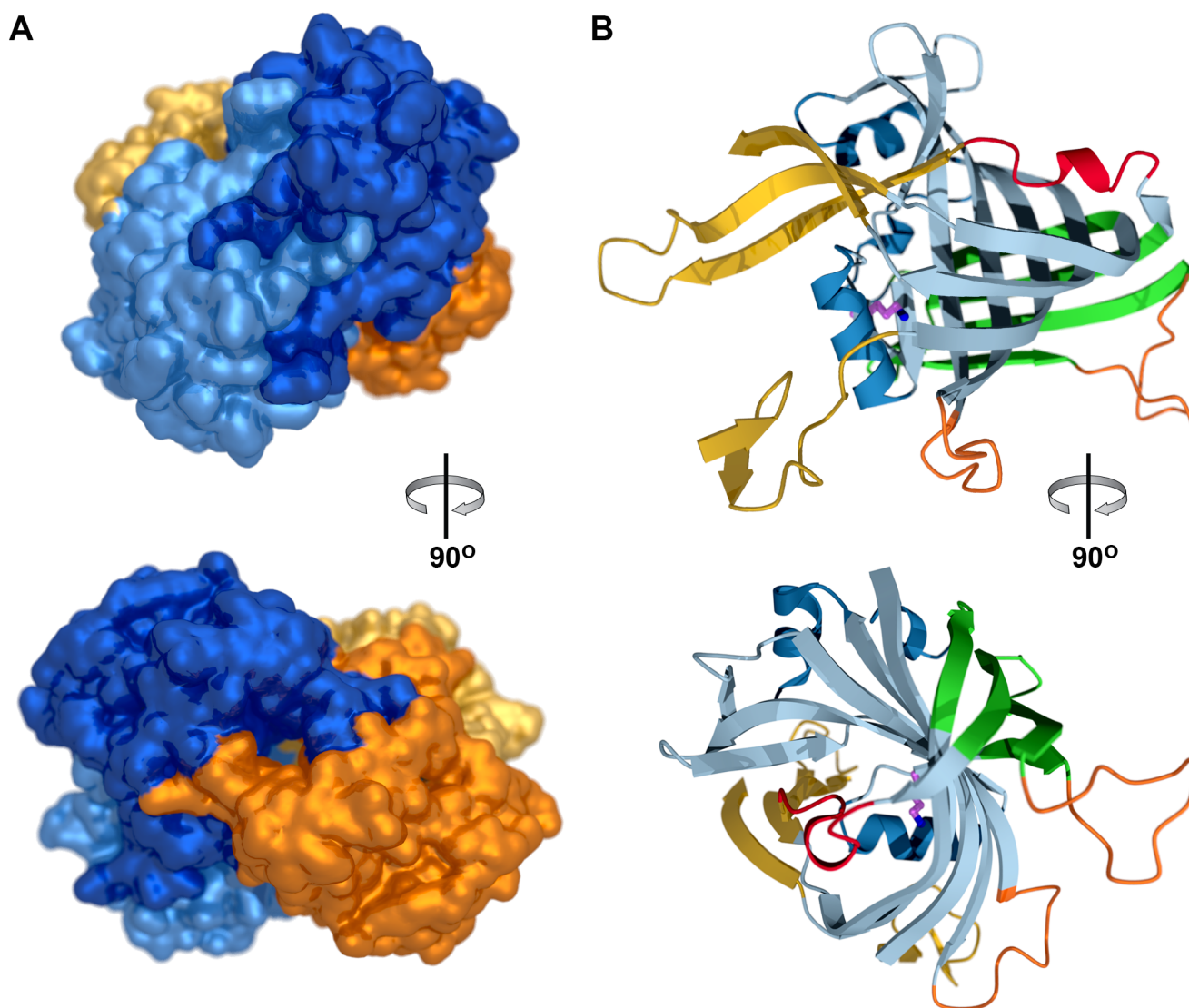


Figure 2. (A) Rendering of the solvent accessible surface of Sbi00515 showing the extensive tetramer interface formed by the long, interdigitating loops (top). This interface is repeated on the back side with the orange and pale yellow protomers. The pair of dimers is held together (bottom) by short loops that appear to "clip" the two dimers together to form the tetramer. (B) The ribbon diagram showing a single protomer is oriented like the dark blue protomer in panel A. The main barrel of the β -cone fold is colored pale blue, with the "side barrel" colored green. The dimer interface loops are colored yellow, and the loops forming the interface between the dimers are colored orange. The section of the polypeptide that is colored red is the "active site loop" that may control access to the active site. The catalytic Lys122 is shown as a ball-and-stick representation with purple carbon atoms.

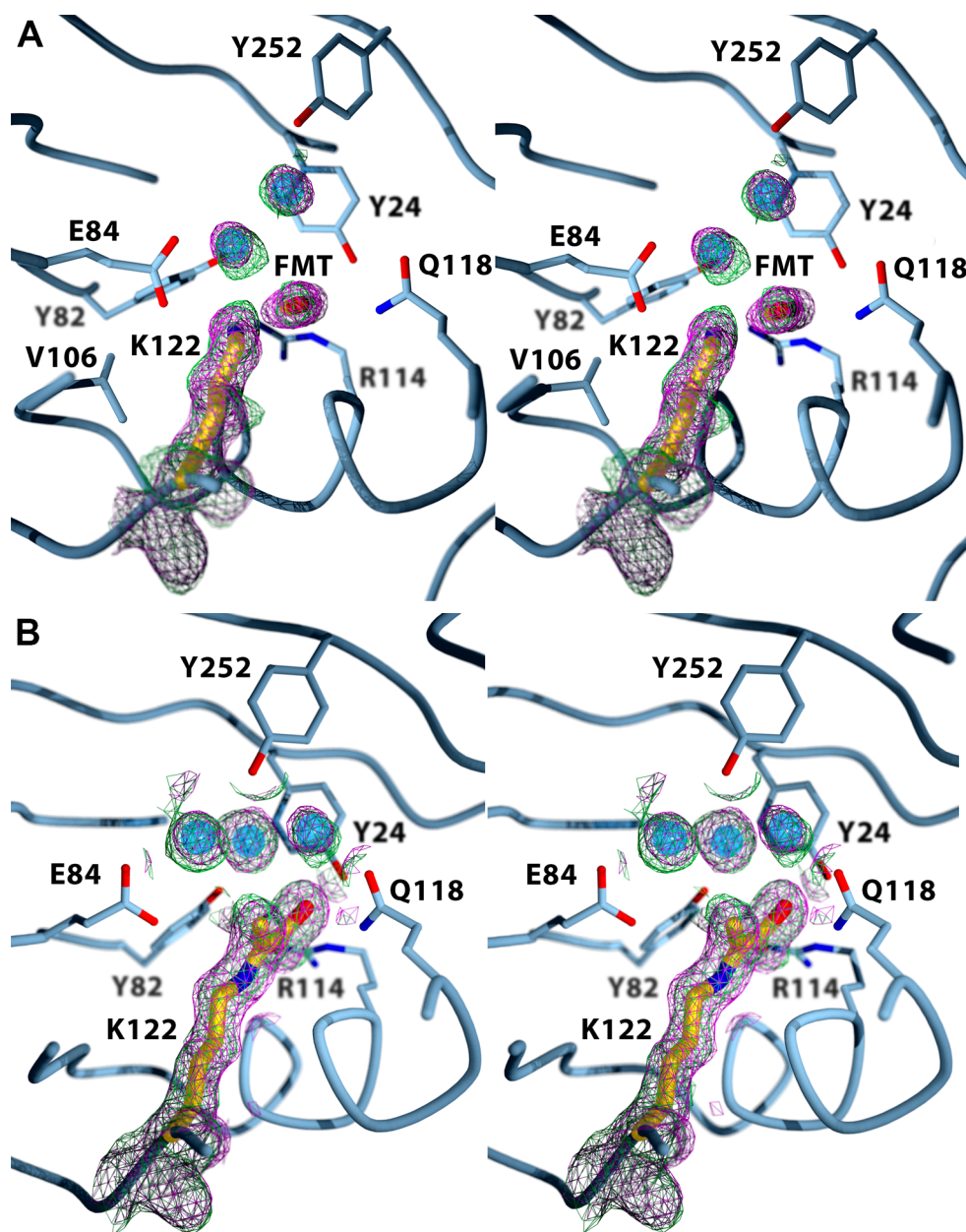


Figure 3. (A) Stereoview of the active site in the “unliganded” Sbi00515 structure showing potassium formate from the crystallization solution bound (refer to Figure 4 for relevant hydrogen bonding interactions and their distances). The position of this formate ion shows that the carboxylate-binding site identified in *S. hygroscopicus* MppR is retained in Sbi00515. The lower water molecule in this view (labeled “1” in Figure 4) bridges Tyr82 and Glu84, suggesting that both residues could participate in the Schiff base chemistry. The upper water molecule (“2” in Figure 4) is held in place by interactions with Tyr252, which is the major difference between the Sbi00515 and ShMppR active sites. (B) The Sbi00515-pyruvate Schiff base complex shows pyruvate covalently bound to the enzyme as indicated by continuous electron density between Lys122 and the α -carbon of pyruvate. The side chain of pyruvate is too short to unequivocally differentiate between the imine and enamine forms of the Schiff base. Note that water “1” has been displaced, water “2” remains in a similar position, and two new water molecules have been recruited so that Glu84, Gln118, and Tyr252 are all linked by an extensive hydrogen bonding network. In both panels, the experimental $2|F_o| - |F_c|$ electron density map (magenta) and the simulated annealing composite omit $2|F_o| - |F_c|$ electron density map (green), both contoured at 1.0σ , are drawn with a 2.0 \AA radius around each atom of Lys122, formate or pyruvate, and select water molecules. This figure and subsequent figures showing crystallographic structures were rendered with the POVSCRIPT³⁴ modification of MOLSCRIPT³⁴ and POVray.

did not react with any of the aldehyde substrates used in this study.

Overall Structure and Comparisons to CaADC and ShMppR. Sbi00515 crystallized in space group $P2_12_12$ with four molecules in the asymmetric unit (unit cell dimensions $a = 157.3 \text{ \AA}$, $b = 123.5 \text{ \AA}$, $c = 53.1 \text{ \AA}$, and $\alpha = \beta = \gamma = 90^\circ$). The asymmetric unit contents are arranged in a tetramer that matches closely the

arrangement seen in ShMppR.⁶ This tetramer is a dimer of dimers (Figure 2A). The “dimer interface” is extensive, being comprised of interdigitating loops (Met1–Pro21 and Arg186–Glu203) that bury 2642 \AA^2 , or 20% of the protomer surface area. The interface between the dimers, which we call the “tetramer interface”, is smaller, burying 1621 \AA^2 , or 12% of the protomer surface, and is also comprised of two surface loops (Ser68–

Gln81 and Gln129–Gly164). The homotetrameric quaternary structure shared by Sbi00515 and ShMppR is markedly different from that of CaADC, which is a homododecamer. In both cases, the trimerization platform of CaADC is occluded by the loops of the tetramer interface. This pair of sequence insertions (see Figure S5 of the Supporting Information) accounts for the difference in quaternary structures between the classical ADCs and the MppR-like family. Thus far, there is no known functional consequence of the quaternary structure in ADCSF enzymes.

The tertiary structure of Sbi00515 is essentially identical to those of both MppR and CaADC, with root-mean-square deviations (rmsds) for all aligned C_α atoms of 1.4 and 1.7 Å, respectively. This is not surprising, given that all ADCSF proteins of known structure {PDB entries 3BH2, 3BH3,³ 4JM3,⁶ 3C8W [Joint Center for Structural Genomics (JCSG), unpublished], and 3CMB (JCSG, unpublished)} share the same β -cone or double-barrel fold first identified by Ho et al.³ (Figure 2B). In spite of the remarkable similarity of the overall folds, the active sites of Sbi00515 and CaADC are different. Specifically, as in ShMppR, Arg29, the residue responsible for orienting the substrate in CaADC, and Glu61, thought to electrostatically encourage the carboxylate group of acetoacetate to leave as CO_2 , are missing in Sbi00515. These two sequence changes alone would account for the loss of acetoacetate decarboxylase activity in the MppR-like enzymes.

The other major difference between CaADC and the MppR-like enzymes is the presence of the very polar “carboxylate-binding site” adjacent to the catalytic lysine residue (Lys122 in Sbi00515). This site is marked in the “unliganded” structure of Sbi00515 by a bound formate ion from the crystallization solution (Figures 3A and 4A). The ion is held by hydrogen bonding interactions between O1 of formate and the hydroxyl group of Tyr24 (2.6 Å) or the guanidinium group of Arg114 (2.7 Å), and between O2 of formate and the amide nitrogen atom of Gln118 (2.9 Å) or the amino group of Lys122 (2.7 Å). Two water molecules are also bound in close proximity of the catalytic Lys122 and the bound formate ion. One, labeled “1” in Figure 4A, is bridging Tyr82 and Glu84 (equidistant at 2.7 Å), while the other, labeled “2,” is held by interactions to water “1” (2.9 Å) and the hydroxyl group of Tyr252 (2.6 Å). The position of water molecule “1,” only 3.3 Å from the amino group of Lys122, suggests that Tyr82 and Glu84 might both participate in the Schiff base chemistry of Lys122.

The active site of Sbi00515 does differ subtly from that of ShMppR, which explains the fact that the latter is able to catalyze the condensation of imidazole-4-carboxaldehyde and pyruvate.⁶ In Sbi00515, Tyr252 replaces the Glu283 of MppR that is thought to help orient the guanidinium group of a hydroxylated arginine derivative for cyclization.⁶ In addition, Tyr82 is a phenylalanine residue in MppR (Phe116), and Tyr24 of Sbi00515 is also a phenylalanine in ShMppR (Phe58). All of the other residues are identical (Figure 5A). Tyr24 of Sbi00515 is especially interesting, because it is a component of the carboxylate-binding site not present in ShMppR and alters the conformation of the Schiff base complex between pyruvate and Lys122.

Schiff Base Complex with Pyruvate. Crystals of Sbi00515 were soaked in a solution containing 30 mM sodium pyruvate, and the resulting covalent imine complex was trapped crystallographically (Figures 3B and 4B). The carboxylate moiety of pyruvate is bound in the carboxylate-binding site of the enzyme, making hydrogen bonding interactions with the hydroxyl groups of Tyr24 and Tyr82 (2.6 and 3.2 Å, respectively) and the amide

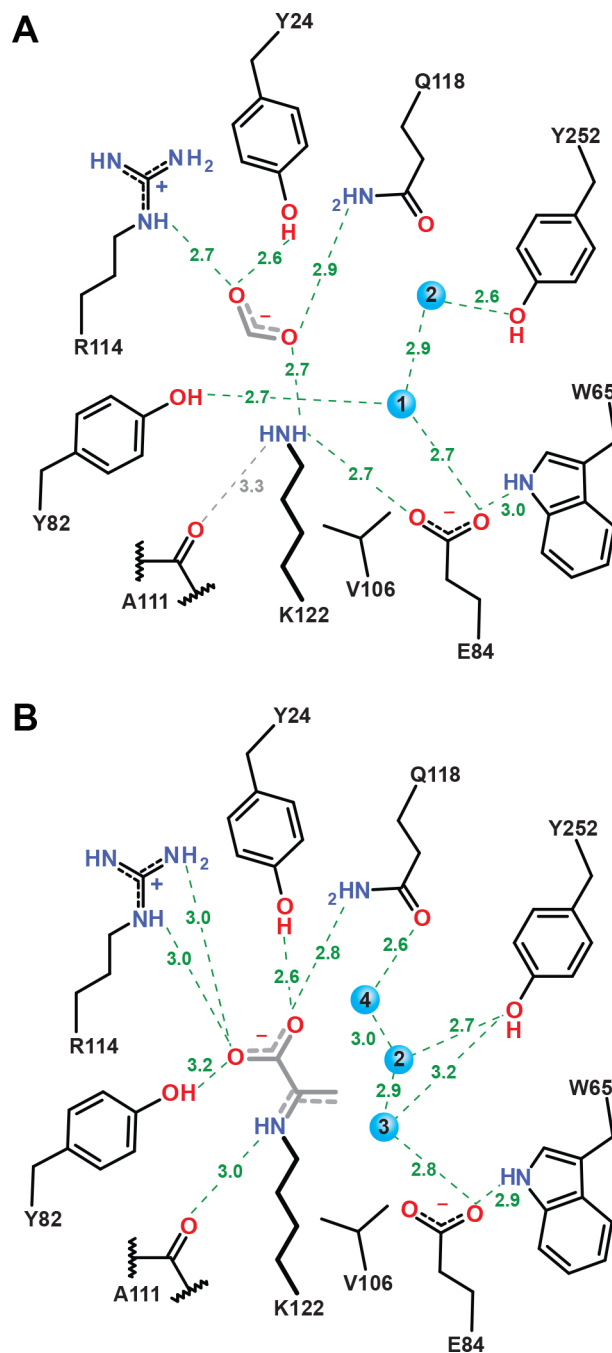


Figure 4. Schematic views of (A) the Sbi00515-formate complex and (B) the Sbi00515-pyruvate complex showing potential hydrogen bonding interactions and their distances (in angstroms).

nitrogen atom of Gln118 (2.8 Å), as well as a potential salt bridge with Arg114 (bidentate at 3.0 Å). Binding of pyruvate does not impact the positions of the side chains comprising the carboxylate-binding site [Tyr24, Arg114, and Gln118 (Figure 5B)], indicating that this site is preconfigured to bind α -keto acids. This may explain, at least in part, why the Schiff base complex is sufficiently stable to be observed in the crystal structure. The residues closer to the catalytic center, Tyr82, Glu84, and Val106, experience small, but significant and concerted, changes in their positions. Tyr82 swings toward the catalytic lysine, moving the hydroxyl group by 0.6 Å, while Glu84 swings away from Lys122, shifting its carboxylate group by 1.4 Å. The distance between the nearest carboxylate O atom of Glu84

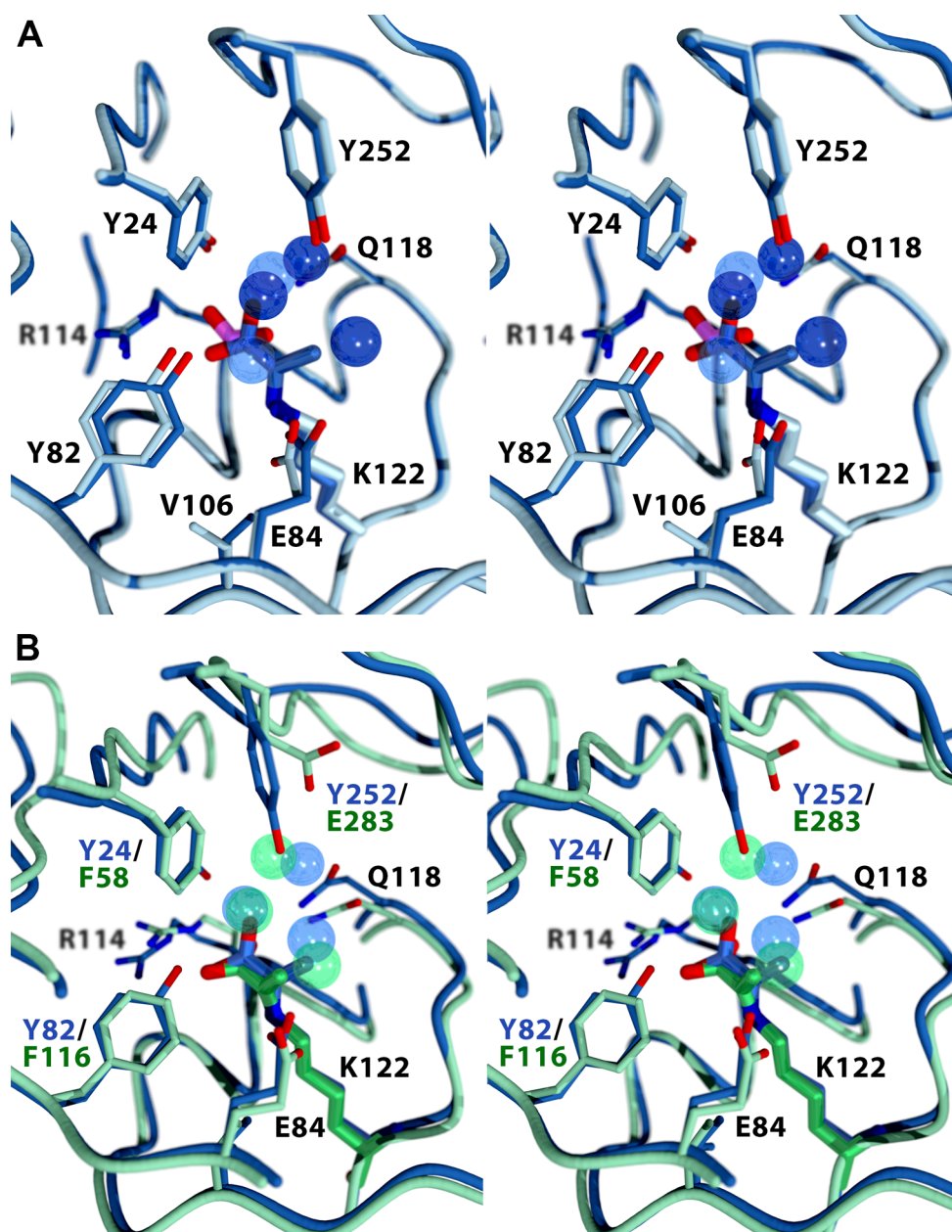


Figure 5. (A) Stereoview showing the complex of Sbi00515 and formate (pale blue model with purple formate ion) overlaid on the enzyme with pyruvate bound (dark blue model). Note the subtle changes in position that occur for residues Tyr82, Glu84, and Tyr252, while the residues comprising the carboxylate-binding site are essentially unperturbed. (B) MppR-pyruvate complex (green model) overlaid on the Sbi00515-pyruvate complex (dark blue model). In spite of the high degree of structural similarity (1.7 Å rmsd for all aligned C α atoms), the arrangement of residues in the carboxylate-binding site is subtly different because of the addition of Tyr24 in Sbi00515. This change results in Sbi00515 binding the pyruvate carboxylate with a monodentate interaction with Arg114 and an additional hydrogen bonding interaction with Tyr24, which holds the carboxylate in plane with the pyruvate methyl group (2.8 Å from CH₃ to carboxylate O). This change, coupled with the Glu \rightarrow Tyr change at position 283/252, may, in part, account for the difference in catalytic activity between Sbi00515 and MppR.

and the pyruvate methyl group is 3.9 Å. Given this arrangement, it is plausible to suggest that Glu84 might act as a general base catalyst to promote formation of the reactive enamine form of the Schiff base. Lastly, although it is some distance from the Lys122-Glu84 dyad, Tyr252 also experiences a 0.6 Å shift of its hydroxyl group toward Lys122, likely because of a rearrangement of the water structure around the catalytic center that occurs upon formation of the Schiff base (Figure 5B). In the pyruvate-bound structure, the water bridging Tyr82 and Glu84 is displaced (water “1” in Figure 4A) and two additional water molecules are recruited (labeled “3” and “4” in Figure 5B) that create a chain

connecting Glu84, Gln118, and Tyr252. The position of water molecule “2” moves along with Tyr252 by 0.8 Å, placing it 3.6 Å from the pyruvate methyl group. The position of this water is instructive, because when the incoming aldehyde substrate is placed so that the aldehyde O atom overlays water “2” and the *re* face of the carbonyl faces the pyruvate methyl group, the distance between the methyl and carbonyl carbons is approximately 3 Å.

It was somewhat surprising to find that although pyruvate occupies the same binding site in Sbi00515 and ShMppR, the conformations of the Schiff base complexes are different. In ShMppR (PDB entry 4JMC), the pyruvate carboxylate group is

nearly coplanar with the guanidinium of Arg148, making a clear salt bridge interaction. In Sbi00515, the substitution of Tyr24 for Phe58 of ShMppR results in the carboxylate-binding site Arg and Gln residues taking different conformations. As a result, the pyruvate carboxylate in the Sbi00515-pyruvate complex is rotated by $\sim 30^\circ$ relative to the ShMppR-pyruvate structure. The rotation of the carboxylate weakens or eliminates the salt bridge to Arg114 and creates a new interaction with Tyr24. This change also forces the carboxylate to nearly eclipse the methyl group ($O2-C1-C2-C3$ torsion angle of 14°). While it is possible that this nearly eclipsed conformation just happens to be the lowest-energy conformation in this complex, the strain inherent in this arrangement, the 2.8 Å distance between the carboxylate oxygen and the methyl carbon, and the potential loss of the salt bridge raise the possibility of substrate-assisted catalysis. It is possible that the carboxylate could abstract a proton from the former pyruvate methyl carbon during the transition from the presumed aldol intermediate to the unsaturated product. A substrate carboxylate is proposed to act as a general acid/base catalyst in sialic acid aldolase.³²

CONCLUSION

The steady state kinetic data presented here show that Sbi00515, a protein of unknown function from *S. bingchengensis*, has *in vitro* pyruvate aldolase-dehydratase activity and is not an acetoacetate decarboxylase as it is currently annotated. This is the first Schiff base-forming aldolase known to use a fold other than the TIM barrel. Given the proximity of the gene encoding Sbi00515 to an uncharacterized polyketide biosynthetic cluster and the strong preference for an unsaturated aldehyde substrate, it is tempting to speculate that Sbi00515 might synthesize an unusual starter or extender unit for the polyketide. However, more detailed genetic and biological studies must be conducted before anything substantive can be concluded in this regard. The structures of the enzyme in complexes with formate and pyruvate point out possible roles of several active site amino acids. Both Tyr82 and Glu84 are near enough to the catalytic lysine residue to make contacts with the presumed hemiaminal intermediate during formation and breakdown of the Schiff base. Because only Glu84 is in a position to reach both Lys122 and the methyl group of pyruvate, and Tyr82 is not absolutely conserved in MppR-like enzymes, Glu84 is the most likely candidate for the general acid/base catalyst. The position of the water molecule held by Y252 in the presence and absence of pyruvate implies that this residue might orient the incoming aldehyde substrate for attack by the enamine nucleophile. Kinetic characterization of active site variants is needed to explore the roles of these residues more deeply. Altogether, these experiments show that there is significant reaction diversity not only in the ADCSF, but also within the MppR-like family itself.

ASSOCIATED CONTENT

Supporting Information

Genomic context of the gene encoding Sbi00515 (Table S1), full NMR spectra of the substrates and reaction products described in the text (Figures S1–S4), and an alignment of Sbi00515, ShMppR, and CaADC (Figure S5). The Supporting Information is available free of charge on the ACS Publications website at DOI: 10.1021/acs.biochem.5b00483.

AUTHOR INFORMATION

Corresponding Author

*Address: 3210 N. Cramer St., Milwaukee, WI 53211. E-mail: silvaggi@uwm.edu. Phone: (414) 229-2647.

Funding

This work was supported by Grant MCB-1157392 from the National Science Foundation, Directorate for Biological Sciences.

Notes

The authors declare no competing financial interest.

ACKNOWLEDGMENTS

Use of the Advanced Photon Source, an Office of Science User Facility operated for the U.S. Department of Energy (DOE) Office of Science by Argonne National Laboratory, was supported by the U.S. DOE under Contract DE-AC02-06CH11357. Use of LS-CAT Sector 21 was supported by the Michigan Economic Development Corp. and the Michigan Technology Tri-Corridor (Grant 08SP1000817).

ABBREVIATIONS

ADC, acetoacetate decarboxylase; ADCSF, acetoacetate decarboxylase-like superfamily; CaADC, *C. acetobutylicum* acetoacetate decarboxylase; PDB, Protein Data Bank; ShMppR, *S. hygroscopicus* MppR.

REFERENCES

- (1) Frey, P. A., Kokesh, F. C., and Westheimer, F. H. (1971) A reporter group at the active site of acetoacetate decarboxylase. I. Ionization constant of the nitrophenol. *J. Am. Chem. Soc.* 93, 7266–7269.
- (2) Highbarger, L. A., Gerlt, J. A., and Kenyon, G. L. (1996) Mechanism of the reaction catalyzed by acetoacetate decarboxylase. Importance of lysine 116 in determining the pKa of active-site lysine 115. *Biochemistry* 35, 41–46.
- (3) Ho, M. C., Menetret, J. F., Tsuruta, H., and Allen, K. N. (2009) The origin of the electrostatic perturbation in acetoacetate decarboxylase. *Nature* 459, 393–397.
- (4) Lederer, F., Coutts, S. M., Laursen, R. A., and Westheimer, F. H. (1966) Acetoacetate decarboxylase. Subunits and properties. *Biochemistry* 5, 823–833.
- (5) Warren, S., Zerner, B., and Westheimer, F. H. (1966) Acetoacetate decarboxylase. Identification of lysine at the active site. *Biochemistry* 5, 817–823.
- (6) Burroughs, A. M., Hoppe, R. W., Goebel, N. C., Sayyed, B. H., Voegtline, T. J., Schwabacher, A. W., Zabriskie, T. M., and Silvaggi, N. R. (2013) Structural and functional characterization of MppR, an enduracididine biosynthetic enzyme from *Streptomyces hygroscopicus*: Functional diversity in the acetoacetate decarboxylase-like superfamily. *Biochemistry* 52, 4492–4506.
- (7) Wang, X. J., Yan, Y. J., Zhang, B., An, J., Wang, J. J., Tian, J., Jiang, L., Chen, Y. H., Huang, S. X., Yin, M., Zhang, J., Gao, A. L., Liu, C. X., Zhu, Z. X., and Xiang, W. S. (2010) Genome sequence of the milbemycin-producing bacterium *Streptomyces bingchengensis*. *J. Bacteriol.* 192, 4526–4527.
- (8) Xiang, W. S., Wang, J. D., Wang, X. J., and Zhang, J. (2007) Two new β -class milbemycins from *Streptomyces bingchengensis*: Fermentation, isolation, structure elucidation and biological properties. *J. Antibiot.* 60, 351–356.
- (9) Xiang, W. S., Wang, J. D., Wang, X. J., Zhang, J., and Wang, Z. (2007) Further new milbemycin antibiotics from *Streptomyces bingchengensis*. Fermentation, isolation, structural elucidation and biological activities. *J. Antibiot.* 60, 608–613.
- (10) Xiang, W. S., Wang, J. D., Fan, H. M., Wang, X. J., and Zhang, J. (2008) New seco-milbemycins from *Streptomyces bingchengensis*: Fermentation, isolation and structure elucidation. *J. Antibiot.* 61, 27–32.

- (11) Wang, X. J., Wang, J. D., Xiang, W. S., and Zhang, J. (2009) Three new milbemycin derivatives from *Streptomyces bingchenggensis*. *J. Asian Nat. Prod. Res.* 11, 597–603.
- (12) Zhang, B. X., Zhang, H., Wang, X. J., Wang, J. D., Liu, C. X., and Xiang, W. S. (2011) New milbemycins from mutant *Streptomyces bingchenggensis* X-4. *J. Antibiot.* 64, 753–756.
- (13) Reimer, M. (1931) Benzalpyruvic Acid Dibromide. *J. Am. Chem. Soc.* 53, 3147–3149.
- (14) Zhu, L. F., Meng, Q. H., Fan, W. Z., Xie, X. M., and Zhang, Z. G. (2010) Direct Asymmetric Hydrogenation of 2-Oxo-4-arylbut-3-enoic Acids. *J. Org. Chem.* 75, 6027–6030.
- (15) Mach, H., Middaugh, C. R., and Lewis, R. V. (1992) Statistical determination of the average values of the extinction coefficients of tryptophan and tyrosine in native proteins. *Anal. Biochem.* 200, 74–80.
- (16) Otwinowski, Z., and Minor, W. (1997) Processing of X-ray Diffraction Data Collected in Oscillation Mode. *Methods Enzymol.* 276, 307–326.
- (17) Battye, T. G., Kontogiannis, L., Johnson, O., Powell, H. R., and Leslie, A. G. (2011) iMOSFLM: A new graphical interface for diffraction-image processing with MOSFLM. *Acta Crystallogr. D* 67, 271–281.
- (18) Leslie, A. G. W. (1992) Recent changes to the MOSFLM package for processing film and image plate data. *Joint CCP4 + ESF-EAMCB Newsletter on Protein Crystallography*, 26.
- (19) Evans, P. (2006) Scaling and assessment of data quality. *Acta Crystallogr. D* 62, 72–82.
- (20) Collaborative Computational Project, No. 4 (1994) The CCP4 suite: Programs for protein crystallography. *Acta Crystallogr. D* 50, 760–763.
- (21) Vonnrhein, C., Blanc, E., Roversi, P., and Bricogne, G. (2007) Automated structure solution with autoSHARP. *Methods Mol. Biol.* 364, 215–230.
- (22) Zwart, P. H., Afonine, P. V., Grosse-Kunstleve, R. W., Hung, L. W., Ioerger, T. R., McCoy, A. J., McKee, E., Moriarty, N. W., Read, R. J., Sacchettini, J. C., Sauter, N. K., Storoni, L. C., Terwilliger, T. C., and Adams, P. D. (2008) Automated structure solution with the PHENIX suite. *Methods Mol. Biol.* 426, 419–435.
- (23) Terwilliger, T. C., Grosse-Kunstleve, R. W., Afonine, P. V., Moriarty, N. W., Zwart, P. H., Hung, L. W., Read, R. J., and Adams, P. D. (2008) Iterative model building, structure refinement and density modification with the PHENIX AutoBuild wizard. *Acta Crystallogr. D* 64, 61–69.
- (24) Emsley, P., Lohkamp, B., Scott, W. G., and Cowtan, K. (2010) Features and development of Coot. *Acta Crystallogr. D* 66, 486–501.
- (25) Afonine, P. V., Mustyakimov, M., Grosse-Kunstleve, R. W., Moriarty, N. W., Langan, P., and Adams, P. D. (2010) Joint X-ray and neutron refinement with phenix.refine. *Acta Crystallogr. D* 66, 1153–1163.
- (26) Word, J. M., Lovell, S. C., Richardson, J. S., and Richardson, D. C. (1999) Asparagine and glutamine: Using hydrogen atom contacts in the choice of side-chain amide orientation. *J. Mol. Biol.* 285, 1735–1747.
- (27) Chen, V. B., Arendall, W. B., III, Headd, J. J., Keedy, D. A., Immormino, R. M., Kapral, G. J., Murray, L. W., Richardson, J. S., and Richardson, D. C. (2010) MolProbity: All-atom structure validation for macromolecular crystallography. *Acta Crystallogr. D* 66, 12–21.
- (28) Urzhumtseva, L., Afonine, P. V., Adams, P. D., and Urzhumtsev, A. (2009) Crystallographic model quality at a glance. *Acta Crystallogr. D* 65, 297–300.
- (29) Moriarty, N. W., Grosse-Kunstleve, R. W., and Adams, P. D. (2009) electronic Ligand Builder and Optimization Workbench (eLBOW): A tool for ligand coordinate and restraint generation. *Acta Crystallogr. D* 65, 1074–1080.
- (30) Sello, G., and Di Gennaro, P. (2013) Aldol reactions of the trans-o-hydroxybenzylidenepyruvate hydratase-aldolase (tHBP-HA) from *Pseudomonas fluorescens* N3. *Appl. Biochem. Biotechnol.* 170, 1702–1712.
- (31) Ferrara, S., Mapelli, E., Sello, G., and Di Gennaro, P. (2011) Characterization of the aldol condensation activity of the trans-o-hydroxybenzylidenepyruvate hydratase-aldolase (tHBP-HA) cloned from *Pseudomonas fluorescens* N3. *Biochim. Biophys. Acta* 1814, 622–629.
- (32) Smith, B. J., Lawrence, M. C., and Barbosa, J. A. (1999) Substrate-Assisted Catalysis in Sialic Acid Aldolase. *J. Org. Chem.* 64, 945–949.
- (33) Fenn, T. D., Ringe, D., and Petsko, G. A. (2003) POVScript+: A program for model and data visualization using persistence of vision ray-tracing. *J. Appl. Crystallogr.* 36, 944–947.
- (34) Kraulis, P. (1991) MOLSCRIPT: A program to produce both detailed and schematic plots of protein structures. *J. Appl. Crystallogr.* 24, 946–950.